

Can We Predict The Human Preference For Text-to-Image Content Prior To Generation And Is It Even Useful To Do So?

Joong Ho Kim

jkim5@lsu.edu

Keith G. Mills

keith.mills@lsu.edu

LSU ATHENA Lab

Baton Rouge, LA, U.S.A. 70803

Abstract

Diffusion Models (DM) have revolutionized text-driven generation by enabling the synthesis of high-quality, photorealistic visual content from user prompts. Whereas prior advances in visual generation such as VAEs and GANs were primarily evaluated on perceptual or visual similarity metrics such as FID PSNR, DM advances have fostered the development of more advanced Human Preference Metrics (HPM) that model and quantify human judgment as scalar values.

However, DMs synthesize content using an inherently stochastic process where random noise seeds generation. The initial random noise directly affects the quality of generated outputs, both qualitatively and quantitatively. This influence is pronounced in smaller models for local deployment scenarios. Given this phenomenon, we first investigate to what extent we can predict scalar HPM scores prior to committing compute resources for generation. Further, we then investigate to what extent we can leverage such prediction to improve the quality of generated images, and also study which HPMs are best suited for this task. Our investigation reveals that not only is this possible, but that it is feasible to achieve negligible hardware overhead. Code is available at <https://github.com/LSU-ATHENA/HPM-Predict>.

Introduction

Diffusion Models (DM) [18] have become the de facto tool for facilitating open-source generation of photorealistic visual content [1, 10] such as images [2] and videos [36, 73] in local deployment scenarios [7]. Whereas prior visual generation models such as Variational AutoEncoders (VAE) [63] and Generative Adversarial Networks (GAN) [19] were primarily evaluated on distance and noise metrics such as the Fréchet Inception Distance (FID) [24] and Peak Signal-to-Noise Ratio (PSNR) [13], Text-to-Image (T2I) DMs such as SDXL [41, 47] and Diffusion Transformers (DiT) [6, 58] excel at generating visual content from textual prompts [23]. These advances in generative performance have given rise to Human Preference Metrics (HPM) [65, 42, 69, 72] which attempt to quantify to what extent a human would find a generative image desirable, given the textual prompt used to generate it.



Figure 1: Illustrating the effect of initial random noise on DM output, both qualitatively and quantitatively. Prompt: “anthropomorphic profile of the white snow owl Crystal priestess...” from [56], generated by Hunyuan-DiT, then scored by ImageReward [72] and HPSv2 [69].

However, DMs use a costly iterative process seeded by random noise which has been shown to affect generated outputs both qualitatively [65] and quantitatively [46, 76], i.e., images, as shown in Figure 1. This motivates a simple question: Can we mitigate the effect of the initial noise on generative quality? Existing techniques in the literature range from examining the interaction between prompt and noise inside the DM cross-attention mechanism [20] to adjusting the initial noise based on the prompt [76] prior to generation to costlier fine-tuning [57] and RLHF-based [17] approaches. However, such approaches overlook the relationship that exists between the initial random noise and the resultant HPM scores corresponding to the image generated by said noise.

This paper answers the question: Given a textual prompt, how can we preemptively choose a better initial noise prior to performing the costly DM generation process that will yield a superior output from a human preference point of view? We answer this question by separately examining the extent to which HPM scores can be estimated from DM initial conditions, whether optimizing based on these estimates can yield superior generative output images, alongside an examination of which human preference metrics are best suited to this task. Our detailed contributions are as follows:

First, we question whether DM initial conditions, i.e., the textual prompt and initial noise, carry sufficient signal information to adequately estimate the HPM scores of the image they would generate. We answer this question by training performance predictors [43, 58] that leverage existing ideas in initial noise optimization [17, 30, 37, 44, 52, 60, 57, 76], such as examining the DM cross-attention map [20], as well as broader literature in low-cost estimators [21, 40] which provides several solutions at varying compute-cost levels. Further, we study the efficacy of different training losses and evaluation metrics for these predictors.

Second, leveraging these findings, we integrate our HPM predictors into existing T2I DM pipelines. Specifically, given the textual prompt, we then apply a simple Best-of-N (BoN) [9, 13] optimization sort using our predictors, then select the best noise to generate an image from. We then measure the HPM scores for this image. This provides a more meaningful evaluation of our preference score predictors by considering to what extent they actually improve the quality of generated outputs. Furthermore, this allows us to measure and compare the compute cost overhead of our predictors in an end-to-end scenario akin to what a real-world user would face.

Third, we provide a lateral study comparing the efficacy of different HPMs [55, 47, 69, 72]. Specifically, we question what human preference metrics are easier to train a predictor on, which lead to better DM outputs when integrated into an end-to-end DM pipeline, as well as which HPMs tend to agree or disagree with each other when examining images generated

via our method compared to a baseline approach.

We conduct extensive experiments on several convolutional U-Net and Transformer [46] DMs such as SDXL [47], DreamShaper [48], Hunyuan-DiT [58] and PixArt- Σ [6]. Across a slew of HPMs such as HPSv2 [59], HPSv3 [42], ImageReward [72] and PickScore [65]. Our results show that it is indeed possible to broadly improve DM generative quality using a human preference performance predictor; however, care must be taken when selecting which preference metrics to train the predictor on, and that simpler predictors that do not rely on the DM at all when performing BoN not only achieve superior average gains, but do so at a significantly reduced computational cost on multiple hardware devices.

2 Background and Related Work

Diffusion Models (DM) [29] are generative AI models that synthesize content such as images [6, 4, 47], videos [8, 72], audio [28], molecules [64], neural network weights [63], etc. [60], by initially sampling a random noise tensor $X_T \sim \mathcal{N}(0, 1)$. Inspired by thermodynamic processes [63], a DM gradually refines X_T using a reverse diffusion process (RDP) over a series of discrete timesteps $t \in [T, \dots, 0]$. There are many forms of RDP equations [12, 62]. For example, one of the simplest RDPs is the Denoising Diffusion Implicit Model (DDIM) RDP [64], formally given by

$$X_{t-1} = \alpha_{t-1} \left(\frac{X_t - \sigma_t \varepsilon_\theta(X_t, t, c)}{\alpha_t} \right) + \sigma_{t-1} \varepsilon_\theta(X_t, t, c), \quad (1)$$

where α_t and σ_t are determined by a pre-defined scheduler and ε_θ is the *denoiser* deep neural network (DNN), typically a large U-Net [64] or Diffusion Transformer (DiT) [46]. After a preset number of iterations, the RDP terminates $t = 0$, yielding the final output X_0 . In the case of traditional DMs [63], X_0 could be a 3-channel $C = 3$ RGB image I with specified height H_I and width W_I .

Latent Diffusion Models (LDM) [48] are largely responsible for the recent popularity in DM research and open-source usage by end-users. LDMs operate by performing prediction in the latent space z of a Variational AutoEncoder (VAE) [63]. In this case, $X_0 = z$ would not be an RGB image with $C = 3$ channels, but would instead be passed through a VAE decoder $g(z)$ in order to generate the final output, i.e., an RGB image $I = g(z) = g(X_0)$. Importantly, $X_T \sim \mathcal{N}(0, 1)$ is still a stochastically sampled tensor for LDMs.

2.1 Text-Driven Diffusion

Text-to-Image (T2I) generation further involves a user-defined textual prompt, i.e., ‘A crocodile in a sweater’ [66]. Specifically, given a prompt p , we first tokenize [49] and encode the prompt into the conditioning matrix $c \in \mathbb{R}^{|p_{tok}| \times d_c}$ where p_{tok} is the tokenized prompt and d_c is the token embedding dimension. The format of the denoiser DNN changes from $\varepsilon_\theta(X_t, t)$ to $\varepsilon_\theta(X_t, t, c)$ to accommodate the prompt conditioning, but the overarching RDP is unchanged as c is constant across all timesteps.

Internally, cross-attention [69] facilitates interaction between the noise X_t and prompt conditioning c , regardless of whether the denoiser ε_θ is a convolutional U-Net [61, 45, 47, 48] or DiT [2, 6, 6, 4, 15]. Specifically, inside the denoiser DNN, the noise tensor is translated into a patch sequence [12] to form the *query* aspect of the attention mechanism;

$Q_X \in \mathbb{R}^{h \times P \times d_h}$ where P is the number of patches while h and d_h are the number of attention heads and head embedding dimension, respectively. Likewise, the prompt conditioning forms the *key* and *value* attention tensors, $K_c, V_c \in \mathbb{R}^{h \times |p_{tok}| \times d_h}$. Thus, the noise and prompt interact to compute the softmax attention map $\text{softmax}(Q_X K_c^T) \in [0, 1]^{h \times P \times |p_{tok}|}$ which determines what prompt tokens each noise patch will attend to and draw information from.

The key source of variability in DMs, especially locally-deployable DMs, is that X_T is stochastically sampled and this randomness is propagated into the query Q_X and cross-attention mechanism. Figure 1 provides a sample illustration, where given the same prompt, i.e., c is held constant, yet different X_T cause drastically different images to form, leading to a qualitatively and quantitatively different outputs. Such an issue is of importance given that the denoiser ε_θ is a large DNN, typically consisting of ranging from 600M parameters [8, 6] to at least several billion [15, 58, 47] parameters that, per the RDP, performs multiple rounds of inference to generate an output whose quality varies with X_T which is not even provided by the user. This motivates the need to quantify the quality of a DM output and attempt to control, mitigate, or optimize in the reality where X_T is stochastic.

2.2 T2I Evaluation via Human Preference Estimation

The goal of T2I generation is to produce an image I which the end-user believes adequately realizes their provided textual prompt p . This objective is easier to describe than execute, as, unlike older visual generation metrics like FID [23], PSNR [13] and CLIPScore [23], human preferences carry a degree of subjectivity and are more difficult to quantify, usually requiring user studies and surveys [8, 9, 43, 47].

However, the advent of T2I DMs has motivated the development of *learned* human preference reward models or Human Preference Metrics (HPM), such as Human Preference Score v2 (HPSv2) [59], HPSv3 [40], ImageReward (IR) [72], PickScore (PS) [55], etc. [75]. Specifically, human preference metrics perform the heavy lifting involved in executing a user study, such as experimental design and participant recruitment. Once the study is complete, the results are further utilized to train a deep neural network (DNN) predictor model $\phi(p, I)$ which receives a user-provided prompt p and T2I-generated image I as input, and then estimates a *human preference score* $S_{p, I} \in \mathbb{R}$. Formally,

$$S_{p, I} = \phi(p, I), \quad (2)$$

where higher $S_{p, I}$ indicates a more preferable image. Recently, these methods have been shown to form a reliable set of benchmarks for accurately evaluating new T2I models [71], as well as performing Reinforcement Learning via Human Feedback (RLHF) [76, 12, 57, 52, 70] and especially for measuring the efficacy of DM efficiency [8, 9] and optimization [49] techniques, such as initial noise optimization [76]. The goal of this paper is to study to what extent we can further leverage these advances to achieve effective initial noise optimization, and how best to do so efficiently, as we next explain.

3 Methodology

In this section we introduce a technique for achieving initial noise optimization via HPM estimation. Figure 2 provides a high-level overview of our technique. We first introduce the high-level idea for a predictor architecture, and then discuss how it can be combined with Best-of-N (BoN) in an existing DM pipeline. Next, we take a finer look at the design of our

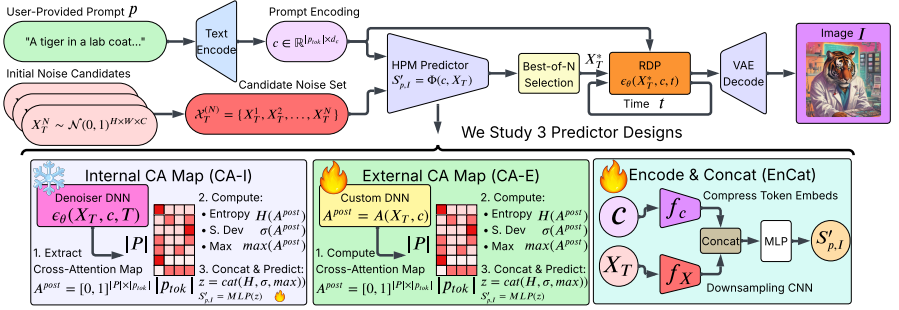


Figure 2: HPM predictor design. Given the DM initial conditions, we consider three types of predictors, abbreviated as CA-I, CA-E and EnCat, which produce $S'_{p,I}$ from c and X_T . **Snowflake** and **flame** denote if model weights are frozen or trainable, respectively.

predictor, specifically emphasizing how to model the interaction of X_T and p , before finally providing an overview of how to train our predictor.

3.1 Human Preference Score Prediction from Initial Conditions

Recall Eq. 2 from Sec. 2.2 which describes how HPMs train a predictor ϕ that maps a given prompt p and image I to a scalar score $S_{p,I}$ as way to model how desirable a human would find the image. In the context of latent T2I DMs, the image is the output of a VAE decoder $I = g(X_0)$ where X_0 is the final output of the iterative reverse diffusion process (RDP) described in Sec. 2. For simplicity, we will use RDP as shorthand for Eq. 1 and as an abstraction for an arbitrary RDP [76, 62], i.e., $X_0 = \text{RDP}(X_T, c)$ where $X_T \sim \mathcal{N}(0, 1)$ is the initial stochastic noise and c is the encoding of prompt p .

Given this setup, we ask a simple question: To what extent can we predict the human preference score $S_{p,I}$ from the DM initial conditions c and X_T and how best can we do so? Given the above, we reformulate the T2I generative and evaluation process as a *scalar regression* prediction problem [21, 68] as follows:

$$S'_{p,I} = \Phi(c, X_T), \quad (3)$$

where Φ is a *new* human preference predictor model that, in contrast to the original ϕ , predicts $S'_{p,I}$, the *estimation* of $S_{p,I}$ given the user-provided textual prompt embedding c and the initial noise X_T utilized to generate an image I , rather than the image itself as ϕ does.

The utility behind this approach is straightforward: Generating an RGB image requires substantial compute, e.g., the large denoiser DNN ε_θ and RDP. This image, the prompt utilized to generate it, will have a corresponding human preference score $S_{p,I}$, and in fact we can re-write the equation for a human preference predictor to include the RDP by making the substitutions $S_{p,I} = \phi(p, I) = \phi(p, g(\text{RDP}(X_T, c)))$ where c is the encoding of p .

This reframing makes the role of the initial stochastic noise X_T on the human preference score $S_{p,I}$ more explicit. Except, whereas an RGB image is a 3D tensor $I \in \mathbb{R}^{3 \times H_I \times W_I}$ that contains many different elements, the number of which scales quadratically with $H_I W_I$, the human preference score for the image I is just a scalar value, $S_{p,I} \in \mathbb{R}$, which, according to information theory, should require less computation to estimate $S'_{p,I}$ [51, 57, 68, 74], i.e., using a smaller predictor [21, 40, 43, 68] model which we denote as Φ in Eq. 3.

Further, although at first glance, predicting HPM scores directly from Gaussian noise may appear unintuitive, in T2I DMs, the interaction between X_T and the prompt encoding c is established at the earliest stages of the RDP via cross-attention [20]. This interaction determines how different regions of the latent representation align with prompt tokens, effectively biasing the trajectory of the RDP. As a result, certain noises are inherently more compatible with a given prompt than others [65], leading to systematic variation in downstream HPM scores. We hypothesize that this early-stage alignment signal is sufficiently informative to enable lightweight predictors $\Phi(c, X_T)$ to approximate the preference score without requiring full image generation. Moreover, should this hold, then we can leverage the reduced cost of Φ compared to $g(\text{RDP}(X_T, c))$ to improve existing DM pipelines in an end-to-end manner.

3.2 Initial Noise Optimization via Best-of-N Sorting

Given a user-provided textual prompt p , a T2I DM encodes it into the tensor $c \in \mathbb{R}^{|p_{\text{tok}}| \times d_c}$ per Sec. 2.1 to condition generation. The user does not select the initial noise, but it is instead randomly sampled; $X_T \sim \mathcal{N}(0, 1)$. Thus, prior to generation, instead of sampling a single initial noise, we can instead sample of *pool* of N candidate noises, $\mathcal{X}_T^{(N)} = \{X_T^1, X_T^2, \dots, X_T^N\}$. Then, we can use our predictor Φ to estimate the human preference score for each noise given the prompt per Eq. 3. This ties a scalar value to each candidate noise, allowing us to perform Best-of-N (BoN) [9, 18] selection by sorting the noises according to the score estimations and then select the noise X_T^* with the highest estimated score:

$$X_T^* = \arg \max_{X_T^{(j)} \in \mathcal{X}_T^{(N)}} \Phi(c, X_T^{(j)}). \quad (4)$$

Then, only the selected noise X_T^* is passed through the full DM RDP to generate an image which we can then evaluate. The idea is that by preemptively optimizing the noise based on the estimated score $S'_{p,I}$, we will generate a more desirable image with a higher actual human preference score $S_{p,I}$.

However, this procedure imposes additional overhead on the already-costly DM RDP. Depending on the exact DNN architecture specification of Φ and choice of N , that overhead can range from a negligible amount to something that has a noticeable impact on end-to-end generation times. Next, we discuss several potential options.

3.3 Preference Predictor Design

Our predictor $\Phi(c, X_T)$ produces an estimate $S'_{p,I}$ of the human preference score $S_{p,I}$ for an image I and prompt p using the prompt conditioning c and initial noise $X_T \sim \mathcal{N}(0, 1)$. The challenge in designing this predictor is two-fold: First, both c and X_T are multi-dimensional tensors whereas $S'_{p,I}$ will be a single scalar value. Second, the accuracy of $S'_{p,I}$, and therefore, its downstream utility per Sec. 3.2 crucially depends on providing sufficient interaction between c and X_T so as to extract as much useful information [61] as possible. In this paper, we highlight three distinct formats of Φ . Figure 2 provides a high-level illustration.

Internal Cross-Attention Mapping. Initial Noise Optimization (InitNO) [20] is one of the earliest works that improves DM generative quality by adjusting X_T . InitNO do not adjust X_T *prior* to generation, but instead apply edits to the DM’s internal cross-attention map from Sec. 2.1. Taking inspiration from this, our first type of predictor receives as input, the first cross-attention map $A^{\text{post}} = \text{softmax}(Q_X K_c^T) \in [0, 1]^{h \times P \times |p_{\text{tok}}|}$ computed by the DM.

We then compress the noise patch dimension P by computing the entropy $A_H^{post} \in \mathbb{R}^{h \times |p_{tok}|}$, standard deviation $A_\sigma^{post} \in \mathbb{R}^{h \times |p_{tok}|}$ and max value $A_{max}^{post} \in [0, 1]^{h \times |p_{tok}|}$ of each row of the attention matrix. Next, for each of these tensors we apply a head compression factor r ; $h \bmod r = 0$, compressing the head dimension from h to h/r by summing each group of r maps. We then flatten the compressed head dimension and concatenate these matrices. This gives rise to a vector $\vec{a} \in \mathbb{R}^{3h/r|p_{tok}|}$ which we feed into a simple multi-layer perceptron (MLP) to produce $S'_{p,I}$. We call this predictor type **Cross-Attention-Internal** or **CA-I** for short.

External Cross-Attention Mapping. Another way to model the interaction between c and X_T is to still rely on a cross-attention map but to manually compute it outside of the DM. Specifically, we apply a streamlined patchify convolution which converts X_T into a patch sequence, positional encoding [14], and a simple cross-attention mechanism which pairs the patched X_T with c . We apply the same set of transformers and reductions to the cross-attention map as CA-I to reduce it from a multi-dimensional tensor down to a vector, and then likewise feed it into an MLP. We dub this type of predictor **Cross-Attention-External** or **CA-E** for short. Unlike CA-I, we do not need to invoke partial inference on the DM to compute the A^{post} used to produce $S'_{p,I}$.

Traditional Encode-and-Concatenate. Finally, we also consider a traditional form of multi-input, multi-modal predictor that encodes each input into a vector, then concatenates them together and feeds the result into an MLP. Specifically, this predictor contains a noise encoder f_X which uses a simple ResNet-style [22] CNN to aggressively downsamples the noise from a 2D tensor into a vector. In parallel, a prompt encoder f_c uses a series of linear layers to progressively shrink the initial prompt token embedding dimension d_c down to 1 to produce a vector of length $|p_{tok}|$. Finally, we concatenate the outputs of f_X and f_c together and feed the resultant vector into an MLP to produce $S'_{p,I}$. We dub this predictor **Encode-and-Concat** or **EnCat** for short.

In the supplementary materials, we provide extensive implementation details and hyper-parameters. Further, we also provide ablation studies comparing how well each of these predictors performs, comparing design, training loss functions and evaluation metrics.

3.4 Training Objective

Regardless of the form our predictor Φ takes, its efficacy when integrated into an existing DM pipeline will depend on the choice of training loss. To simplify this choice, we consider a differentiable ranking/information retrieval loss paired with a traditional regression loss. This is formally given by

$$\mathcal{L}_\Phi = \mathcal{L}_{rank} + \mathcal{L}_{reg}, \quad (5)$$

where \mathcal{L}_{rank} is either the Lambdaloss [56] or a differentiable Spearman Rank Correlation Coefficient (SRCC) [9] loss computed over a given training batch, and \mathcal{L}_{reg} is a regression loss, typically the Mean Absolute Error (MAE); $\mathcal{L}_{reg} = |S_{p,I} - S'_{p,I}|$.

4 Results

In this section, we present our experimental setup and results. We structure our results around three research questions (RQ):

- **RQ1:** Given only the DM initial conditions, the prompt encoding c and stochastic noise X_T , can we accurately estimate the human preference score $S_{p,I}$ using a predictor $\Phi(c, X_T)$? Further, if this is possible, how is this estimation best achieved?
- **RQ2:** By pairing our predictor $\Phi(c, X_T)$ with a simple Best-of-N (BoN) sort to optimize X_T prior to generation, can we increase the quality of generated outputs compared to an unoptimized baseline?
- **RQ3:** Which HPMs should we aim to estimate? That is, if we compare different metrics, are some of them easier to predict or better for downstream noise optimization?

To answer these questions, we consider several popular T2I DMs. First, we consider the 2.6B parameter U-Net SDXL [47], a very common base model in the open-source T2I scene that has given rise to many popular fine-tunes [11, 61, 45] such as DreamShaper [40], which we also consider. In terms of DiTs, we consider the lightweight 600M parameter PixArt- Σ [6] as well as the larger 1.6B parameter Hunyuan [68]. For each of these DMs, we use the default checkpoint and hyperparameters from the HuggingFace Diffusers [60] library to generate 1024×1024 resolution images.

In terms of metrics we consider Human Preference Score v2 (HPSv2) [69], HPSv3 [42], ImageReward (IR) [72] and PickScore (PS) [63]. Specifically, we train our predictor Φ on one of these, but then evaluate the end-to-end pipeline performance by generating images from different sets of prompts and using these metrics to judge the human preference for the generated images. In terms of downstream evaluation prompts, we consider two sets of prompts: First, following Golden Noise [74], we consider the first 100 Pick-a-Pick validation set prompts as well as the larger HPSv2 benchmark, which contains 3.2k prompts spread over 4 categories.

4.1 RQ1: Can Initial Conditions Predict Human Preference?

First, we consider whether it is feasible to estimate human preference scores $S_{p,I}$ for a given HPM from the initial prompt c and noise X_T . For each DM, we train several predictors Φ on tuples of prompt-noise-score $(c, X_T, S_{p,I})$ data. Following [74], we sample 5k prompts from the Pick-a-Pick [65] training dataset and generate 20 initial noises per prompt, for 100k tuples in total per DM. We partition each dataset 80%/10%/10% into disjoint train-validation-test sets along prompt indices; i.e, the prompts themselves are disjoint with respect to our dataset partitions. Following Sec. 3.4 we train using Eq. 5 on MAE and LambdaLoss, while reserving the differentiable SRCC for the supplementary. We also vary our measurements across two separate HPMs: HPSv2, and PickScore. Additional training details can be found in the supplementary.

Table 1 reports our results. Between the choice of DM, predictor training target and evaluation metric, there are 24 trials and EnCat achieves the best performance over half the time (15), and the second best performance in a significant number of the remaining trials (7). However, with exception to Hunyuan, the EnCat encoder contains significantly more parameters than both the CA-I and CA-E predictors. Ironically, the CA-E predictor, which externally computes the cross-attention map always contains the fewest number of parameters, yet is arguably the 2nd best design by predictor metrics, as it achieves the best and second best results more frequently than CA-I. Overall, these results demonstrate that it is indeed feasible to predict human preference scores $S_{p,I}$ from initial conditions. The question is whether accurate prediction entails improvement in generative quality.

Table 1: Human preference predictor performance on DM initial conditions. We experiment across 4 DMs and use 2 HPMs as targets. For each DM and target, we train a CA-I, CA-E and EnCat predictor with on the LambdaLoss and MAE. We then evaluate the NDCG@3, NDCG@5 and MAE on the held-out test set and also report the predictor parameters. **Best** and *second best* results in **bold** and *italics*, respectively.

Model	Target	Predictor	Params	NDCG@3 (\uparrow)	NDCG@5 (\uparrow)	MAE (\downarrow)
SDXL	HPSv2	CA-I	1.33M	<i>0.592</i>	0.594	0.035
		CA-E	1.11M	0.589	<i>0.614</i>	0.038
		EnCat	3.50M	0.599	0.628	<i>0.036</i>
	PickScore	CA-I	1.33M	<i>0.570</i>	0.607	1.243
		CA-E	1.11M	0.566	<i>0.614</i>	<i>0.899</i>
		EnCat	3.50M	0.609	0.625	0.811
DreamShaper	HPSv2	CA-I	1.33M	0.595	0.626	0.037
		CA-E	1.11M	0.612	<i>0.640</i>	<i>0.028</i>
		EnCat	3.50M	<i>0.608</i>	0.647	0.026
	PickScore	CA-I	1.33M	<i>0.588</i>	<i>0.627</i>	1.179
		CA-E	1.11M	0.580	0.614	<i>1.001</i>
		EnCat	3.50M	0.590	0.630	0.971
Hunyuan-DiT	HPSv2	CA-I	8.33M	0.594	0.622	<i>0.035</i>
		CA-E	1.48M	0.589	0.626	0.024
		EnCat	3.59M	<i>0.591</i>	<i>0.625</i>	0.024
	PickScore	CA-I	8.33M	0.585	0.624	1.201
		CA-E	1.48M	0.576	0.611	<i>0.981</i>
		EnCat	3.59M	<i>0.580</i>	<i>0.620</i>	0.872
PixArt- Σ	HPSv2	CA-I	7.52M	0.581	0.617	0.035
		CA-E	2.09M	0.586	<i>0.619</i>	<i>0.031</i>
		EnCat	12.01M	0.583	0.620	0.030
	PickScore	CA-I	7.52M	<i>0.564</i>	<i>0.604</i>	1.242
		CA-E	2.09M	0.575	0.614	<i>1.016</i>
		EnCat	12.00M	0.554	0.595	0.979

Table 2: Comparison of regression prediction and downstream HPM results on DreamShaper. We use MAE+LambdaLoss to train each predictor, varying the HPM from PickScore to HPSv2. The final column reports the downstream generation score corresponding to the target metric. ‘Standard’ is an unoptimized baseline without using a predictor. Best and second best results in **bold** and *italics*, respectively.

Model	Target	Method	MAE+LambdaLoss		Downstream
			NDCG@5	SRCC	Target Score
Dreamshaper	PickScore	Standard	–	–	22.6041
		CA-I	0.6266	0.2327	22.6096
		CA-E	<i>0.6135</i>	<i>0.5637</i>	22.6238
		EnCat	0.6295	0.5901	<i>22.6146</i>
	HPSv2	Standard	–	–	0.3461
CA-I		0.6255	0.1614	0.3456	
CA-E		<i>0.6397</i>	<i>0.6756</i>	0.3467	
EnCat		0.6467	0.7337	<i>0.3464</i>	

Further, Table 2 provides this result for DreamShaper. Specifically, we integrate our predictors into the existing DM pipeline and use the BoN sorting from Sec. 3.2 with $N = 100$ to generate images. We then measure the score $S_{p,l}$ for these images according to the source HPM the predictor trained on

(i.e., PickScore on top, HPSv2 on bottom). We then report the average score across all prompts. We compare this to a baseline ‘Standard’ that does not utilize BoN sorting at all. In contrast, both CA-E and EnCat achieve respectable SRCC despite training on LambdaLoss and also consistently outperform the standard baseline.

4.2 RQ2: Does Predictor-Guided Noise Selection Improve $S_{p,l}$?

We further evaluate whether offline prediction translates into improved image generation on other HPMs. Specifically, given our LambdaLoss+MAE predictors trained on either HPSv2 or PickScore, we further consider whether the improvements on the source metric utilized to

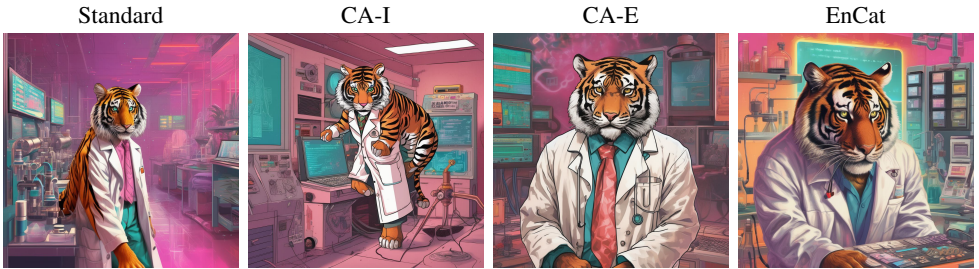
Table 3: Downstream Best-of-N evaluation using predictor-guided initial noise selection with $N = 100$. We report aligned evaluations: HPSv2-trained predictors on HPSv2 benchmark prompts and PickScore-trained predictors on PickScore/Pick-a-Pic prompts. Higher is better for all metrics. Best and second-best results within each model, target, and prompt set are shown in **bold** and *italics*, respectively.

Model	Target	Dataset	Method	HPSv2	HPSv3	ImageReward	PickScore
Hunyuan-DiT	HPSv2	HPSv2	Standard	0.3146	11.8764	1.0782	22.5782
			CA-I	<i>0.3157</i>	11.8274	1.0817	22.5668
			CA-E	0.3165	11.9431	<i>1.0950</i>	22.5790
			EnCat	0.3162	<i>11.8807</i>	1.0996	22.5918
	PickScore	PickScore	Standard	0.3043	7.3080	0.8778	21.8130
			CA-I	0.3025	7.3220	0.8819	21.8508
			CA-E	<i>0.3069</i>	7.8130	0.9361	21.8163
			EnCat	0.3086	<i>7.5530</i>	<i>0.8912</i>	21.8836
DreamShaper	HPSv2	HPSv2	Standard	0.3461	13.8647	1.3152	23.7061
			CA-I	0.3456	13.8820	1.3094	23.6733
			CA-E	0.3467	<i>13.9103</i>	1.3191	23.7084
			EnCat	<i>0.3464</i>	13.9292	<i>1.3181</i>	23.7201
	PickScore	Pick-a-Pic	Standard	0.3251	9.2526	1.0202	22.6041
			CA-I	0.3224	9.2587	<i>1.0626</i>	22.6096
			CA-E	<i>0.3296</i>	9.3564	1.0491	22.6238
			EnCat	0.3332	<i>9.3111</i>	1.0757	<i>22.6146</i>
SDXL	HPSv2	HPSv2	Standard	0.2869	<i>10.5942</i>	<i>0.8506</i>	22.5161
			CA-I	0.2865	10.5408	0.8575	<i>22.5166</i>
			CA-E	<i>0.2871</i>	10.5515	0.8399	22.5051
			EnCat	0.2888	10.6055	0.8447	22.5177
	PickScore	PickScore	Standard	0.2840	6.6744	0.5794	21.6467
			CA-I	<i>0.2866</i>	6.9240	0.5733	<i>21.6788</i>
			CA-E	0.2848	6.8311	<i>0.5955</i>	21.7104
			EnCat	0.2879	<i>6.8435</i>	0.6419	21.6777
PixArt- Σ	HPSv2	HPSv2	Standard	0.3010	12.3826	1.0335	22.6759
			CA-I	0.2994	12.3722	1.0327	22.6911
			CA-E	<i>0.3041</i>	<i>12.4000</i>	1.0363	22.6964
			EnCat	0.3049	12.4401	<i>1.0355</i>	22.6894
	PickScore	PickScore	Standard	0.2976	<i>8.1384</i>	0.8013	21.7987
			CA-I	0.2973	7.9863	0.8614	21.7339
			CA-E	0.2981	8.1271	0.7880	21.7875
			EnCat	<i>0.2980</i>	8.2353	<i>0.8557</i>	<i>21.7971</i>

train the predictor translate to other metrics in a zero-shot sense. In other words, we would ask ‘If we train a predictor on PickScore, does that also translate into $S_{p,I}$ gains for HPSv2, HPSv3 or ImageReward?’

Table 3 reports our findings, which are largely positive. The results show that predictor-guided selection can improve generated images, but the gains depend on both the predictor family and the reward model used for evaluation. Across the aligned settings, EnCat and CA-E are the most consistently competitive designs that most consistently outperform the standard baseline across numerous combinations of DMs, predictor targets and preference metrics. EnCat often improves PickScore oriented evaluations, while CA-E frequently improves HPSv2 or HPSv3 evaluations. In contrast, CA-I is less consistent, falls behind CA-E and EnCat and often struggles to even outperform the baseline.

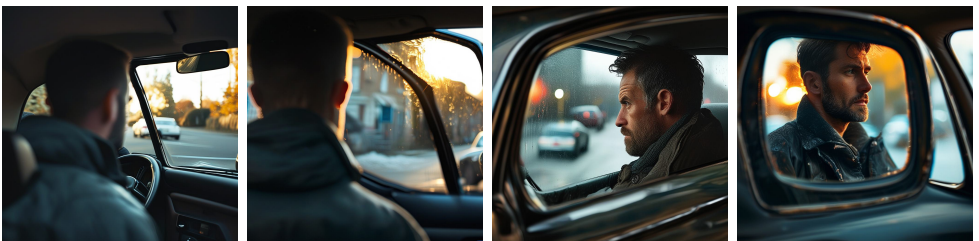
Across the HPMs, we find that HPSv2, HPSv3 and PickScore largely agree with each other. Typically, if one predictor design is best on one of these metrics, it is also the best, or second best, on the others. By contrast, ImageReward stands as the most disagreeable HPM, as it is not uncommon for one predictor like CA-I or the baseline to perform well on it, yet stumble on the other metrics. We further analyze this phenomenon in Section 4.3.



SDXL: “A tiger in a lab coat with a 1980s Miami vibe, turning a well oiled science content machine, digital art.”



Hunyuan-DiT: “A woman lies down surrounded by piles of paintings by Greg Rutkowski.”



PixArt-Σ: “A mans reflection in a side view mirror.”

Figure 3: Qualitative visual examples. DM and prompt details provided. We provide further examples in the supplementary materials.

Next, Figure 3 shows qualitative examples on several DMs. Each row fixes a DM, prompt and then shows the image produced by each method: the ‘Standard’ baseline and then our predictor architectures. For the SDXL prompt, EnCat and CA-E render a clear tiger in a lab coat with a detailed laboratory, while CA-I produces an awkward full body pose and the standard image is less detailed. For the Hunyuan-DiT prompt, EnCat shows the woman lying down amid piles of paintings on the floor, while the other selection seat the subject upright or keep the paintings hung on the wall. For the PixArt- Σ prompt, EnCat frames the man’s reflected face inside the side mirror and CA-E shows his face through the window, while the standard and CA-I images show him from behind with no visible reflection. Overall, these examples align with Table 3: The CA-E and EnCat predictor architectures are better at downstream BoN noise optimization.

4.3 RQ3: Which Preference Metrics are Suitable for Optimization?

We now perform a lateral comparison of the different HPMs considered in this paper. The goal is to quantify to what extent performing initial noise optimization using our predictor Φ on one preference metric will translate to other preference metrics.

To do this, we consider the images generated by our SDXL predictors trained on HPSv2 using LambdaLoss+MAE for the 100 images in the Pick-a-Pick validation set. For each generated image, we compare the score of the predictor-selected output against the standard diffusion baseline under HPSv2, HPSv3, ImageReward, and PickScore. We then count how often a method improves over the standard baseline under individual metrics, pairs of metrics, triples of metrics, and all four metrics. This agreement-based view is useful because each reward model captures a different approximation of human preference, and a method that improves only one metric may not correspond to a broadly preferred output.

Table 4 tallies the results. The single-metric rows show that all three predictors can improve over the standard baseline under HPSv2, HPSv3, and PickScore for at least half of the prompts. However, that is not the case when considering ImageReward (IR), which deems the standard baseline image to be superior more than half the time for each predictor.

These results further cascade when we consider groups of two-or-more HPMs at once and establish a clear pattern: Whenever ImageReward is factored in, judgment is skewed towards the standard baseline. This is not the case for when we pair either HPSv2 or v3 with PS, or consider all three of them together. This is further borne out in Figure 4 for the prompt “Four dogs on the street”:

Table 4: Metric-agreement counts for SDXL HPSv2-trained predictors on 100 Pick-a-Pic validation set prompts. Each row reports the number of prompts, out of 100, for which the predictor-selected image improves over the Standard baseline under every metric in the listed set. Single metrics, pairs, triples, and all-four agreement are separated by horizontal rules.

Human Preference Metrics	CAM-I	CAM-E	EnCat
HPSv2	52	55	58
HPSv3	54	57	61
PS	50	53	56
IR	39	41	43
HPSv2 + HPSv3	37	40	43
HPSv2 + PS	35	38	41
HPSv3 + PS	36	39	42
HPSv2 + IR	26	28	30
HPSv3 + IR	25	27	29
PS + IR	23	25	27
HPSv2 + HPSv3 + PS	29	32	34
HPSv2 + HPSv3 + IR	18	20	22
HPSv2 + PS + IR	17	19	21
HPSv3 + PS + IR	16	18	20
All	12	14	16





Standard	CA-I	CA-E	EnCat
			
HPSv2 0.2581	HPSv2 0.2981	HPSv2 0.3398	HPSv2 0.3379
HPSv3 5.6969	HPSv3 9.1720	HPSv3 10.9810	HPSv3 12.9293
IR 1.0351	IR 1.6239	IR 1.4739	IR 0.6849
PS 22.6994	PS 24.9392	PS 24.5920	PS 24.4301

Figure 4: Qualitative example for the preference-metric analysis on the prompt “Four dogs on the street.” **Bold** marks the best method per metric.

EnCat and CA-E render the requested four dogs and top HPSv2 and HPSv3, yet ImageReward ranks EnCat the lowest of all methods, below the Standard baseline. PickScore stands as a bit of an outlier, ranking CA-I the highest even though it only renders three dogs, but we nevertheless note that the PS score values for CA-E and EnCat are much closer to CA-I than they are to the Standard baseline.

Further, among the predictor families, EnCat and CA-E generally preserve higher agreement counts than CA-I. This is consistent with our prior results: CA-I can occasionally improve a metric, but it is less reliable when agreement across multiple preference models is required. Overall, these results suggest that HPSv2 and PickScore are more suitable training targets for this task than ImageReward, since improvements under them more often transfer to other preference metrics. Finally, the corresponding PickScore-trained agreement table is provided in the supplementary material.

4.4 Computational Cost Across Hardware

Table 5: Params and FLOPs comparison for predictor-guided Best-of- N with $N = 1$. We separate predictor FLOPs from the FLOPs required to perform feature extraction of the cross-attention map for CA-I (FE FLOPs). ‘D.S.’ shorthand for DreamShaper.

Diffusion Model	Method	Params	Predictor FLOPs	FE FLOPs	Total FLOPs
SDXL/D.S.	CA-I	1.33M	2.70M	13.5T	13.5T
	CA-E	1.11M	489M	0	489M
	EnCat	3.50M	432M	0	432M
Hunyuan-DiT	CA-I	8.33M	16.7M	30.1T	30.1T
	CA-E	1.64M	1.09G	0	1.09G
	EnCat	3.63M	1.86G	0	1.86G
PixArt- Σ	CA-I	7.52M	15.0M	13.3T	13.3T
	CA-E	2.09M	1.33G	0	1.33G
	EnCat	12.00M	6.71G	0	6.71G

Next, we measure the computational overhead introduced by guided noise selection when integrated into a DM pipeline. Table 5 provides a view of predictor FLOPs where we separate FLOPs required by the HPM predictor

itself, from feature-extraction FLOPs. Here, the true weakness of CA-I becomes clearer: The FLOPs cost required to perform partial inference on the DM denoiser to extract the cross-attention map raises the overall cost of evaluating a *single* noise X_T by several magni-

Table 6: Runtime comparison for predictor-guided noise optimization across varying Nvidia hardware. We consider BoN selection time for $N = 100$ as well as total generation time for the DM to generate an image. All results in seconds. Recall that CA-I utilizes the internal cross-attention map from the first DM transformer block when $t = T$.

GPU Device	Diffusion Model	Method	Selection Time	+Generation
A100	SDXL/DreamShaper	Standard	0	6.3651
		CA-I	13.8529	20.0833
		CA-E	0.0763	6.3680
		EnCat	0.0669	6.3648
	Hunyuan-DiT	Standard	0	17.863
		CA-I	43.5509	61.331
		CA-E	0.123	17.9027
		EnCat	0.1069	17.8880
	PixArt- Σ	Standard	0	17.1243
		CA-I	65.4173	77.3544
		CA-E	4.3579	16.6388
		EnCat	4.8550	16.8888
RTX PRO 5000	SDXL/DreamShaper	Standard	0	5.4108
		CA-I	10.3342	15.5247
		CA-E	0.0201	5.1992
		EnCat	0.044	5.1811
	Hunyuan-DiT	Standard	0	15.3909
		CA-I	34.7874	50.4423
		CA-E	0.0493	15.7822
		EnCat	0.0615	15.2791
	PixArt- Σ	Standard	0	9.7646
		CA-I	34.533	41.0288
		CA-E	2.483	8.9693
		EnCat	2.5451	9.1638
DGX Spark	SDXL/DreamShaper	Standard	0	20.4274
		CA-I	40.9684	60.2145
		CA-E	0.0904	19.5241
		EnCat	0.083	19.0025
	Hunyuan-DiT	Standard	0	60.4956
		CA-I	137.3244	196.7365
		CA-E	0.2662	59.7327
		EnCat	0.1966	59.4129
	PixArt- Σ	Standard	0	8.2562
		CA-I	38.9267	45.3572
		CA-E	0.5166	6.9824
		EnCat	0.803	7.2272

tudes - from gigaFLOPs to teraFLOPs - above what is required by CA-E and EnCat.

Further, Table 6 provides a complementary view of the wall-clock time consumed to perform BoN selection with $N = 100$ across a trio of hardware devices. As we can see, both CA-E and EnCat add negligible overhead across all DMs and hardware. The issue is CA-I [10], which is substantially more expensive as it must partially invoke the DM denoiser to extract the first cross-attention map at $t = T$. This cost is especially true for the newer DiTs Hunyuan and PixArt- Σ , where selection time for CA-I can exceed the actual generation time multiple times over, but is also of significant concern for SDXL-based U-Nets.

Thus, given the hardware results presented and prior evaluation results, we observe that

CA-I is the least optimal form of predictor for initial noise optimization via human preference estimation. In contrast, both CA-E and EnCat have roughly comparable hardware costs and are around equally capable when it comes to downstream inference in an end-to-end DM pipeline. Notably, these two predictor styles are lightweight and impose limited negligible computational overhead cost.

5 Conclusion

This paper questions whether it is possible to improve T2I DM generative performance by combining human preference metrics, initial noise optimization and Best-of-N (BoN) sorting. We address this with three research questions targeting the feasibility of estimating human preference metrics from DM initial conditions, whether initial optimization via a predictor and BoN can yield downstream improvements on existing DM pipelines, while also performing a lateral comparison of different preference metrics.

To answer these questions, we consider three distinct forms of predictor that models the human preference score from the prompt and initial noise. We find that two of these predictor designs are able to consistently improve end-to-end human preference metric benchmark scores even in a zero-shot setting. Ironically, we also find that the computationally inefficient form of predictor is the least effective at this task.

References

- [1] AUTOMATIC1111. Stable diffusion webui. <https://github.com/AUTOMATIC1111/stable-diffusion-webui>, 2022.
- [2] Black Forest Labs. Flux. <https://github.com/black-forest-labs/flux>, 2024.
- [3] Mathieu Blondel, Olivier Teboul, Quentin Berthet, and Josip Djolonga. Fast differentiable sorting and ranking. In *International Conference on Machine Learning*, pages 950–959. PMLR, 2020.
- [4] Bradley Brown, Jordan Juravsky, Ryan Ehrlich, Ronald Clark, Quoc V Le, Christopher Ré, and Azalia Mirhoseini. Large language monkeys: Scaling inference compute with repeated sampling. *arXiv preprint arXiv:2407.21787*, 2024.
- [5] Junsong Chen, Jincheng Yu, Chongjian Ge, Lewei Yao, Enze Xie, Zhongdao Wang, James T. Kwok, Ping Luo, Huchuan Lu, and Zhenguo Li. Pixart- α : Fast training of diffusion transformer for photorealistic text-to-image synthesis. In *The Twelfth International Conference on Learning Representations, ICLR 2024, Vienna, Austria, May 7-11, 2024*. OpenReview.net, 2024. URL <https://openreview.net/forum?id=eAKmQP3m1>.
- [6] Junsong Chen, Chongjian Ge, Enze Xie, Yue Wu, Lewei Yao, Xiaozhe Ren, Zhongdao Wang, Ping Luo, Huchuan Lu, and Zhenguo Li. PixArt- Σ : Weak-to-strong training of diffusion transformer for 4k text-to-image generation. In *European Conference on Computer Vision*, pages 74–91. Springer, 2025.

- [7] Junsong Chen, Shuchen Xue, Yuyang Zhao, Jincheng Yu, Sayak Paul, Junyu Chen, Han Cai, Song Han, and Enze Xie. Sana-sprint: One-step diffusion with continuous-time consistency distillation. In *Proceedings of the IEEE/CVF International Conference on Computer Vision*, pages 16185–16195, 2025.
- [8] Ruichen Chen, Keith G. Mills, Liyao Jiang, Chao Gao, and Di Niu. Re-ttention: Ultra sparse visual generation via attention statistical reshape. In *NeurIPS*, 2025.
- [9] Ruichen Chen, Keith G Mills, and Di Niu. Fp4dit: Towards effective floating point quantization for diffusion transformers. *arXiv preprint arXiv:2503.15465*, 2025.
- [10] ComfyUI Contributors. Comfyui: A node-based gui for stable diffusion, 2025. URL <https://github.com/Comfy-Org/ComfyUI>.
- [11] Cyberdelia. CyberRealistic Pony - | Stable Diffusion XL Checkpoint | Civitai — civitai.com. <https://civitai.com/models/443821/cyberrealistic-pony>, 2026. [Accessed 02-03-2026].
- [12] Giannis Daras, Hyungjin Chung, Chieh-Hsin Lai, Yuki Mitsufuji, Jong Chul Ye, Peyman Milanfar, Alexandros G Dimakis, and Mauricio Delbracio. A survey on diffusion models for inverse problems. *arXiv preprint arXiv:2410.00083*, 2024.
- [13] Chao Dong, Chen Change Loy, and Xiaoou Tang. Accelerating the super-resolution convolutional neural network. In *European conference on computer vision*, pages 391–407. Springer, 2016.
- [14] Alexey Dosovitskiy, Lucas Beyer, Alexander Kolesnikov, Dirk Weissenborn, Xiaohua Zhai, Thomas Unterthiner, Mostafa Dehghani, Matthias Minderer, Georg Heigold, Sylvain Gelly, Jakob Uszkoreit, and Neil Houlsby. An image is worth 16x16 words: Transformers for image recognition at scale. In *9th International Conference on Learning Representations, ICLR 2021, Virtual Event, Austria, May 3-7, 2021*. OpenReview.net, 2021. URL <https://openreview.net/forum?id=YicbFdNTTy>.
- [15] Patrick Esser, Sumith Kulal, Andreas Blattmann, Rahim Entezari, Jonas Müller, Harry Saini, Yam Levi, Dominik Lorenz, Axel Sauer, Frederic Boesel, Dustin Podell, Tim Dockhorn, Zion English, and Robin Rombach. Scaling rectified flow transformers for high-resolution image synthesis. In *Forty-first International Conference on Machine Learning, ICML 2024, Vienna, Austria, July 21-27, 2024*. OpenReview.net, 2024. URL <https://openreview.net/forum?id=FPnUhsQJ5B>.
- [16] Luca Eyring, Shyamgopal Karthik, Karsten Roth, Alexey Dosovitskiy, and Zeynep Akata. Reno: Enhancing one-step text-to-image models through reward-based noise optimization. *Advances in Neural Information Processing Systems*, 37:125487–125519, 2024.
- [17] Luca Eyring, Shyamgopal Karthik, Alexey Dosovitskiy, Nataniel Ruiz, and Zeynep Akata. Noise hypernetworks: Amortizing test-time compute in diffusion models. *arXiv preprint arXiv:2508.09968*, 2025.
- [18] Amirhosein Ghasemabadi, Keith G Mills, Baochun Li, and Di Niu. Guided by gut: Efficient test-time scaling with reinforced intrinsic confidence. *arXiv preprint arXiv:2505.20325*, 2025.

- [19] Ian Goodfellow, Jean Pouget-Abadie, Mehdi Mirza, Bing Xu, David Warde-Farley, Sherjil Ozair, Aaron Courville, and Yoshua Bengio. Generative adversarial nets. In *Advances in neural information processing systems*, pages 2672–2680, 2014.
- [20] Xiefan Guo, Jinlin Liu, Miaomiao Cui, Jiankai Li, Hongyu Yang, and Di Huang. Initno: Boosting text-to-image diffusion models via initial noise optimization. In *Proceedings of the IEEE/CVF Conference on Computer Vision and Pattern Recognition*, pages 9380–9389, 2024.
- [21] Fred X. Han, Keith G. Mills, Fabian Chudak, Parsa Riahi, Mohammad Salameh, Jialin Zhang, Wei Lu, Shangling Jui, and Di Niu. *A General-Purpose Transferable Predictor for Neural Architecture Search*, pages 721–729. Society for Industrial and Applied Mathematics, 2023. doi: 10.1137/1.9781611977653.ch81. URL <https://epubs.siam.org/doi/abs/10.1137/1.9781611977653.ch81>.
- [22] Kaiming He, Xiangyu Zhang, Shaoqing Ren, and Jian Sun. Identity mappings in deep residual networks. In *European Conference on Computer Vision*, pages 630–645. Springer, 2016.
- [23] Jack Hessel, Ari Holtzman, Maxwell Forbes, Ronan Le Bras, and Yejin Choi. CLIP-Score: A reference-free evaluation metric for image captioning. In Marie-Francine Moens, Xuanjing Huang, Lucia Specia, and Scott Wen-tau Yih, editors, *Proceedings of the 2021 Conference on Empirical Methods in Natural Language Processing*, pages 7514–7528, Online and Punta Cana, Dominican Republic, November 2021. Association for Computational Linguistics. doi: 10.18653/v1/2021.emnlp-main.595. URL <https://aclanthology.org/2021.emnlp-main.595/>.
- [24] Martin Heusel, Hubert Ramsauer, Thomas Unterthiner, Bernhard Nessler, and Sepp Hochreiter. Gans trained by a two time-scale update rule converge to a local nash equilibrium. *Advances in neural information processing systems*, 30, 2017.
- [25] Jonathan Ho and Tim Salimans. Classifier-free diffusion guidance. *arXiv preprint arXiv:2207.12598*, 2022.
- [26] Jonathan Ho, Ajay Jain, and Pieter Abbeel. Denoising diffusion probabilistic models. *Advances in neural information processing systems*, 33:6840–6851, 2020.
- [27] Jonathan Ho, Tim Salimans, Alexey Gritsenko, William Chan, Mohammad Norouzi, and David J Fleet. Video diffusion models. *Advances in Neural Information Processing Systems*, 35:8633–8646, 2022.
- [28] Rongjie Huang, Jiawei Huang, Dongchao Yang, Yi Ren, Luping Liu, Mingze Li, Zhenhui Ye, Jinglin Liu, Xiang Yin, and Zhou Zhao. Make-an-audio: Text-to-audio generation with prompt-enhanced diffusion models. In *International Conference on Machine Learning*, pages 13916–13932. PMLR, 2023.
- [29] Liyao Jiang, Ruichen Chen, Chao Gao, and Di Niu. Raise: Requirement-adaptive evolutionary refinement for training-free text-to-image alignment, 2026. URL <https://arxiv.org/abs/2603.00483>.

- [30] Adhithyan Kalaivanan, Zheng Zhao, Jens Sjölund, and Fredrik Lindsten. Ess-flow: Training-free guidance of flow-based models as inference in source space. *arXiv preprint arXiv:2510.05849*, 2025.
- [31] KandooAI. Juggernaut XL - Ragnarok_by_RunDiffusion | Stable Diffusion XL Checkpoint | Civitai — civitai.com. <https://civitai.com/models/133005/juggernaut-xl>, 2025. [Accessed 27-01-2026].
- [32] Tero Karras, Miika Aittala, Timo Aila, and Samuli Laine. Elucidating the design space of diffusion-based generative models. *Advances in neural information processing systems*, 35:26565–26577, 2022.
- [33] Diederik P. Kingma and Max Welling. Auto-encoding variational bayes. In Yoshua Bengio and Yann LeCun, editors, *2nd International Conference on Learning Representations, ICLR 2014, Banff, AB, Canada, April 14-16, 2014, Conference Track Proceedings*, 2014. URL <http://arxiv.org/abs/1312.6114>.
- [34] Alexander Kirillov, Ross Girshick, Kaiming He, and Piotr Dollár. Panoptic feature pyramid networks. In *Proceedings of the IEEE/CVF Conference on Computer Vision and Pattern Recognition*, pages 6399–6408, 2019.
- [35] Yuval Kirstain, Adam Polyak, Uriel Singer, Shahbuland Matiana, Joe Penna, and Omer Levy. Pick-a-pic: An open dataset of user preferences for text-to-image generation. *Advances in neural information processing systems*, 36:36652–36663, 2023.
- [36] Weijie Kong, Qi Tian, Zijian Zhang, Rox Min, Zuozhuo Dai, Jin Zhou, Jiangfeng Xiong, Xin Li, Bo Wu, Jianwei Zhang, et al. Hunyuanvideo: A systematic framework for large video generative models. *arXiv preprint arXiv:2412.03603*, 2024.
- [37] Zeming Li, Xiangyue Liu, Xiangyu Zhang, Ping Tan, and Heung-Yeung Shum. Noisear: Autoregressing initial noise prior for diffusion models. *arXiv preprint arXiv:2506.01337*, 2025.
- [38] Zhimin Li, Jianwei Zhang, Qin Lin, Jiangfeng Xiong, Yanxin Long, Xinchu Deng, Yingfang Zhang, Xingchao Liu, Minbin Huang, Zedong Xiao, Dayou Chen, Jiajun He, Jiahao Li, Wenyue Li, Chen Zhang, Rongwei Quan, Jianxiang Lu, Jiabin Huang, Xiaoyan Yuan, Xiaoxiao Zheng, Yixuan Li, Jihong Zhang, Chao Zhang, Meng Chen, Jie Liu, Zheng Fang, Weiyang Wang, Jinbao Xue, Yangyu Tao, Jianchen Zhu, Kai Liu, Sihuan Lin, Yifu Sun, Yun Li, Dongdong Wang, Mingtao Chen, Zhichao Hu, Xiao Xiao, Yan Chen, Yuhong Liu, Wei Liu, Di Wang, Yong Yang, Jie Jiang, and Qinglin Lu. Hunyuan-dit: A powerful multi-resolution diffusion transformer with fine-grained chinese understanding, 2024.
- [39] Ilya Loshchilov and Frank Hutter. Decoupled weight decay regularization. In *7th International Conference on Learning Representations, ICLR 2019, New Orleans, LA, USA, May 6-9, 2019*. OpenReview.net, 2019. URL <https://openreview.net/forum?id=Bkg6RiCqY7>.
- [40] Shun Lu, Yu Hu, Peihao Wang, Yan Han, Jianchao Tan, Jixiang Li, Sen Yang, and Ji Liu. Pinat: A permutation invariance augmented transformer for nas predictor. In *Proceedings of the AAAI Conference on Artificial Intelligence (AAAI)*, 2023.

- [41] Lykon. Dreamshaper - stable diffusion fine-tune. <https://civitai.com/models/4384/dreamshaper>, 2023.
- [42] Yuhang Ma, Xiaoshi Wu, Keqiang Sun, and Hongsheng Li. Hpsv3: Towards wide-spectrum human preference score. In *Proceedings of the IEEE/CVF International Conference on Computer Vision*, pages 15086–15095, 2025.
- [43] Keith G. Mills, Mohammad Salameh, Ruichen Chen, Wei Hassanpour, Negar Lu, and Di Niu. Qua²sedimo: Quantifiable quantization sensitivity of diffusion models. In *AAAI*, 2025.
- [44] Kiyong Om, Kyuil Sim, Taeyoung Yun, Hyeongyu Kang, and Jinkyoo Park. Posterior inference in latent space for scalable constrained black-box optimization. *arXiv preprint arXiv:2507.00480*, 2025.
- [45] ONOMAAI. Illustrious XL 2.0 - v2.0 | Illustrious Checkpoint | Civitai — civitai.com. <https://civitai.com/models/1369089/illustrious-xl-20>, 2025. [Accessed 27-01-2026].
- [46] William Peebles and Saining Xie. Scalable diffusion models with transformers. In *Proceedings of the IEEE/CVF International Conference on Computer Vision*, pages 4195–4205, 2023.
- [47] Dustin Podell, Zion English, Kyle Lacey, Andreas Blattmann, Tim Dockhorn, Jonas Müller, Joe Penna, and Robin Rombach. SDXL: improving latent diffusion models for high-resolution image synthesis. In *The Twelfth International Conference on Learning Representations, ICLR 2024, Vienna, Austria, May 7-11, 2024*. OpenReview.net, 2024. URL <https://openreview.net/forum?id=di52zR8xgf>.
- [48] Robin Rombach, Andreas Blattmann, Dominik Lorenz, Patrick Esser, and Björn Ommer. High-resolution image synthesis with latent diffusion models. In *CVPR*, 2022.
- [49] Mohammad Salameh, Keith G. Mills, Negar Hassanpour, Fred Han, Shuting Zhang, Wei Lu, Shangling Jui, Chunhua Zhou, Fengyu Sun, and Di Niu. Autogo: Automated computation graph optimization for neural network evolution. In *Advances in Neural Information Processing Systems*, 2023.
- [50] Saurabh Saxena, Charles Herrmann, Junhwa Hur, Abhishek Kar, Mohammad Norouzi, Deqing Sun, and David J Fleet. The surprising effectiveness of diffusion models for optical flow and monocular depth estimation. *Advances in Neural Information Processing Systems*, 36:39443–39469, 2023.
- [51] Claude Elwood Shannon. A mathematical theory of communication. *The Bell system technical journal*, 27(3):379–423, 1948.
- [52] Henry D Smith, Nathaniel L Diamant, and Brian L Trippe. Calibrating generative models. *arXiv preprint arXiv:2510.10020*, 2025.
- [53] Jascha Sohl-Dickstein, Eric Weiss, Niru Maheswaranathan, and Surya Ganguli. Deep unsupervised learning using nonequilibrium thermodynamics. In *International conference on machine learning*, pages 2256–2265. PMLR, 2015.

- [54] Jiaming Song, Chenlin Meng, and Stefano Ermon. Denoising diffusion implicit models. *arXiv preprint arXiv:2010.02502*, 2020.
- [55] Bedionita Soro, Bruno Andreis, Hayeon Lee, Wonyong Jeong, Song Chong, Frank Hutter, and Sung Ju Hwang. Diffusion-based neural network weights generation. *arXiv preprint arXiv:2402.18153*, 2024.
- [56] PixArt-Alpha Team. Pixart-alpha prompt list. <https://github.com/PixArt-alpha/PixArt-alpha/blob/master/asset/samples.txt>, 2024. Accessed: 2026-01-15.
- [57] Naftali Tishby and Noga Zaslavsky. Deep learning and the information bottleneck principle. In *2015 IEEE Information Theory Workshop (ITW)*, pages 1–5. Ieee, 2015.
- [58] Naftali Tishby, Fernando C Pereira, and William Bialek. The information bottleneck method. *arXiv preprint physics/0004057*, 2000.
- [59] Ashish Vaswani, Noam Shazeer, Niki Parmar, Jakob Uszkoreit, Llion Jones, Aidan N Gomez, Łukasz Kaiser, and Illia Polosukhin. Attention is all you need. In I. Guyon, U. Von Luxburg, S. Bengio, H. Wallach, R. Fergus, S. Vishwanathan, and R. Garnett, editors, *Advances in Neural Information Processing Systems*, volume 30. Curran Associates, Inc., 2017. URL https://proceedings.neurips.cc/paper_files/paper/2017/file/3f5ee243547dee91fbd053c1c4a845aa-Paper.pdf.
- [60] Siddarth Venkatraman, Mohsin Hasan, Minsu Kim, Luca Scimeca, Marcin Sendera, Yoshua Bengio, Glen Berseth, and Nikolay Malkin. Outsourced diffusion sampling: Efficient posterior inference in latent spaces of generative models. *arXiv preprint arXiv:2502.06999*, 2025.
- [61] Patrick von Platen, Suraj Patil, Anton Lozhkov, Pedro Cuenca, Nathan Lambert, Kashif Rasul, Mishig Davaadorj, Dhruv Nair, Sayak Paul, William Berman, Yiyi Xu, Steven Liu, and Thomas Wolf. Diffusers: State-of-the-art diffusion models. <https://github.com/huggingface/diffusers>, 2022.
- [62] Bram Wallace, Meihua Dang, Rafael Rafailov, Linqi Zhou, Aaron Lou, Senthil Purushwalkam, Stefano Ermon, Caiming Xiong, Shafiq Joty, and Nikhil Naik. Diffusion model alignment using direct preference optimization. In *Proceedings of the IEEE/CVF Conference on Computer Vision and Pattern Recognition (CVPR)*, pages 8228–8238, June 2024.
- [63] Chaoqi Wang, Guodong Zhang, and Roger Grosse. Picking winning tickets before training by preserving gradient flow. *arXiv preprint arXiv:2002.07376*, 2020.
- [64] Liang Wang, Chao Song, Zhiyuan Liu, Yu Rong, Qiang Liu, and Shu Wu. Diffusion models for molecules: A survey of methods and tasks. *arXiv preprint arXiv:2502.09511*, 2025.
- [65] Ruoyu Wang, Huayang Huang, Ye Zhu, Olga Russakovsky, and Yu Wu. The silent assistant: Noisequery as implicit guidance for goal-driven image generation. In *Proceedings of the IEEE/CVF International Conference on Computer Vision*, pages 17618–17628, 2025.

- [66] Xuanhui Wang, Cheng Li, Nadav Golbandi, Michael Bendersky, and Marc Najork. The lambdaloss framework for ranking metric optimization. In *Proceedings of the 27th ACM international conference on information and knowledge management*, pages 1313–1322, 2018.
- [67] Zifan Wang, Alice Harting, Matthieu Barreau, Michael M Zavlanos, and Karl H Johansson. Source-guided flow matching. *arXiv preprint arXiv:2508.14807*, 2025.
- [68] Colin White, Arber Zela, Robin Ru, Yang Liu, and Frank Hutter. How powerful are performance predictors in neural architecture search? *NeurIPS*, 2021.
- [69] Xiaoshi Wu, Yiming Hao, Keqiang Sun, Yixiong Chen, Feng Zhu, Rui Zhao, and Hongsheng Li. Human preference score v2: A solid benchmark for evaluating human preferences of text-to-image synthesis. *arXiv preprint arXiv:2306.09341*, 2023.
- [70] Ziyi Wu, Anil Kag, Ivan Skorokhodov, Willi Menapace, Ashkan Mirzaei, Igor Gilitschenski, Sergey Tulyakov, and Aliaksandr Siarohin. Densdpo: Fine-grained temporal preference optimization for video diffusion models. *Advances in Neural Information Processing Systems*, 38:171632–171668, 2026.
- [71] Enze Xie, Junsong Chen, Junyu Chen, Han Cai, Haotian Tang, Yujun Lin, Zhekai Zhang, Muyang Li, Ligeng Zhu, Yao Lu, and Song Han. SANA: efficient high-resolution text-to-image synthesis with linear diffusion transformers. In *The Thirteenth International Conference on Learning Representations, ICLR 2025, Singapore, April 24-28, 2025*. OpenReview.net, 2025. URL <https://openreview.net/forum?id=N8Oj1XhtYZ>.
- [72] Jiazheng Xu, Xiao Liu, Yuchen Wu, Yuxuan Tong, Qinkai Li, Ming Ding, Jie Tang, and Yuxiao Dong. Imagereward: Learning and evaluating human preferences for text-to-image generation. *Advances in Neural Information Processing Systems*, 36:15903–15935, 2023.
- [73] Zhuoyi Yang, Jiayan Teng, Wendi Zheng, Ming Ding, Shiyu Huang, Jiazheng Xu, Yuanming Yang, Wenyi Hong, Xiaohan Zhang, Guanyu Feng, Da Yin, Yuxuan Zhang, Weihan Wang, Yean Cheng, Bin Xu, Xiaotao Gu, Yuxiao Dong, and Jie Tang. Cogvideox: Text-to-video diffusion models with an expert transformer. 2025. URL <https://openreview.net/forum?id=LQzN6TRFg9>.
- [74] Andrew Zammit-Mangion, Matthew Sainsbury-Dale, and Raphaël Huser. Neural methods for amortized inference. *Annual Review of Statistics and Its Application*, 12(1): 311–335, 2025.
- [75] Sixian Zhang, Bohan Wang, Junqiang Wu, Yan Li, Tingting Gao, Di Zhang, and Zhongyuan Wang. Learning multi-dimensional human preference for text-to-image generation. In *Proceedings of the IEEE/CVF Conference on Computer Vision and Pattern Recognition (CVPR)*, pages 8018–8027, June 2024.
- [76] Zikai Zhou, Shitong Shao, Lichen Bai, Shufei Zhang, Zhiqiang Xu, Bo Han, and Zeke Xie. Golden noise for diffusion models: A learning framework. In *Proceedings of the IEEE/CVF International Conference on Computer Vision*, pages 17688–17697, 2025.

Supplementary Materials

We provide additional implementation and training details, architecture specifications for each predictor, baseline implementation details, further ablation studies, and additional qualitative image samples.

A Additional Implementation Details

We provide further details on how we train our three predictor families—CA-I, CA-E, and EnCat (Sec. 3.3)—along with their architecture specifications and the implementation of the standard baseline.

A.1 Training Details

Dataset. Each predictor is fit to a per-DM, per-target corpus of 100k examples, assembled by drawing 5k Pick-a-Pic [65] training prompts and pairing every prompt with 20 independently sampled Gaussian noise tensors. Every resulting image is scored by the target reward model in advance, so training consumes precomputed scalars and never invokes the generator. To make the predictor inputs cheap to load, we also precompute and cache each prompt embedding (from the DM’s own text encoder) and its noise tensors to disk. We partition the 100k examples 80%/10%/10% at the prompt level, so a prompt never spans two splits. Targets are standardized to zero mean and unit variance using statistics from the training split only; we store these statistics in the checkpoint to recover native units at inference.

Grouped batching. Since the ranking term acts within a prompt, a batch must contain several noises that share the same prompt. We therefore assemble each batch from $k=12$ prompts at a time; with ~ 20 noises available per prompt this yields ~ 240 examples per batch, supplying enough same-prompt pairs for the within-group ranking objective to be well defined.

Loss function. For our main results we instantiate the ranking–regression objective of Eq. 5 with $\text{LambdaLoss}@5$ [66] as the ranking term and the MAE between predicted and normalized scores as the regression term, weighting the regression term by $\alpha = 0.05$. Since each training prompt has 20 candidate noises, $\text{LambdaLoss}@5$ optimizes the top quarter of the within-prompt candidate list. For the SRCC variant studied in the ablations (Sec. B.1), we instead use the differentiable SRCC of Blondel *et al.* [9] as the ranking term, computed *per prompt group* and averaged over groups within the batch (regularization strength 10^{-2}), again combined with MAE.

Optimization. Predictors are optimized with AdamW [49] (learning rate 10^{-4} , weight decay 10^{-8}) under gradient-norm clipping at 1.0. The learning rate is halved whenever the validation primary metric does not improve for five consecutive epochs. Training runs for at most 80 epochs, and we retain the epoch that maximizes that metric (NDCG for LambdaLoss runs, SRCC otherwise).

Validation metrics. We track three quantities on the held-out validation prompts. A global Spearman correlation (SRCC) summarizes how well the predicted scores order the entire validation pool, while per-prompt $\text{NDCG}@K$ ($K \in \{3, 5\}$), macro-averaged across prompts, checks whether the noises ranked highest within each prompt are the correct ones. We additionally report MAE in de-normalized units to capture absolute regression error.

A.2 Predictor Architectures

CA-I. We read the first internal cross-attention map and reduce each attention row to per-head, per-token entropy, standard deviation, and maximum statistics. A head compression factor r ($h \bmod r = 0$) sums adjacent groups of r heads, reducing the head dimension from h to h/r ; the flattened statistics ($h/r \cdot |p_{tok}| \cdot n_{stat}$) feed the same MLP head as EnCat. The main configuration uses all three statistics with $r=1$.

CA-E. A patchify convolution ($P_k=4$) maps the latent to a patch sequence; a linear layer projects prompt tokens to dimension 256; an 8-head cross-attention block attends patches to prompt tokens. The attention map is reduced to entropy statistics with head compression $r=2$ and scored by the same MLP head, without invoking the diffusion model.

EnCat. The noise encoder is a lightweight convolutional network that downsamples the $4 \times 128 \times 128$ latent to a 1024-d vector. In parallel, the text encoder applies a shared per-token MLP that maps each prompt-token embedding to a scalar, producing a length- $|p_{tok}|$ vector. The two vectors are concatenated and passed to a small MLP head (hidden widths 512, 256, 64; SiLU activations; dropout 0.1) that outputs the scalar score. The embedding dimension d_c and sequence length $|p_{tok}|$ follow each DM’s native text encoder.

A.3 Baseline Implementation

The standard baseline runs the Diffusers [64] pipeline with no noise selection. We seed the noise generator from each prompt’s integer index and apply this same seeding rule to every method, so the baseline and all predictors observe an identical candidate-noise sequence for a given prompt.

B Additional Ablation Studies

This section collects the ablations behind our design and data choices: the per-predictor configuration sweeps (Sec. B.1), the fixed-budget prompt/noise study (Sec. B.2), and the metric-agreement counts for PickScore-trained predictors (Sec. B.3).

B.1 Predictor Configuration Ablations

We sweep the design choices for each predictor under the MAE+SRCC objective and retrain the selected configuration under the main-paper LambdaLoss objective for the results in the main text. The configuration used in the main paper is indicated in each table’s caption.

CA-I. Table 7 sweeps the attention statistic set and head compression on SDXL and PixArt- Σ ; we use entropy+std+max with $r=1$.

CA-E. Table 8 sweeps the statistic set, head compression, and patch size; we use entropy-only with $P_k=4$ and $r=2$.

B.2 Prompt/Noise Allocation

Table 9 allocates a fixed 100K-sample training budget between prompt diversity and per-prompt noise coverage. We train an EnCat predictor on SDXL with the PickScore target under the LambdaLoss@5+0.05MAE objective, split prompts by ID, and select on NDCG@10. For each budget we report offline NDCG@5, NDCG@10, SRCC, and MAE (in the native PickScore scale) on the held-out test split.

Table 7: CA-I internal cross-attention configuration ablation, trained with MAE+SRCC. We vary the attention statistic set (E: entropy; Esm: entropy+std+max) and the head compression $r \in \{1, 2\}$. Bold marks the configuration used in the main paper (Esm, $r=1$). MAE is in each target’s native score scale.

Model	Target	Config	Params	SRCC	NDCG@3	NDCG@5	MAE	
SDXL	HPSv2	E, $r=1$	0.54M	0.098	0.594	0.622	0.0331	
		E, $r=2$	0.34M	0.133	0.584	0.608	0.0330	
		Esm, $r=1$	1.33M	-0.023	0.578	0.608	0.0331	
		Esm, $r=2$	0.74M	0.019	0.579	0.610	0.0333	
PickScore	PickScore	E, $r=1$	0.54M	0.350	0.576	0.603	1.119	
		E, $r=2$	0.34M	0.311	0.573	0.601	1.120	
		Esm, $r=1$	1.33M	0.279	0.562	0.593	1.121	
		Esm, $r=2$	0.74M	0.349	0.572	0.602	1.119	
PixArt- Σ	HPSv2	E, $r=1$	2.61M	0.087	0.567	0.596	0.0348	
		E, $r=2$	1.38M	0.016	0.569	0.599	0.0349	
		Esm, $r=1$	7.52M	0.108	0.566	0.596	0.0348	
		Esm, $r=2$	3.83M	0.165	0.565	0.595	0.0349	
	PickScore	PickScore	E, $r=1$	2.61M	0.009	0.547	0.579	1.242
			E, $r=2$	1.38M	-0.010	0.537	0.575	1.242
			Esm, $r=1$	7.52M	0.069	0.548	0.579	1.243
			Esm, $r=2$	3.83M	0.024	0.548	0.580	1.245

Table 8: CA-E external patch cross-attention configuration ablation, trained with MAE+SRCC. We vary the attention statistic set (E: entropy; Esm: entropy+std+max), the patch size $P_k \in \{4, 8, 16\}$, and the head compression r . The configuration used in the main paper is E, $P_k=4$, $r=2$. MAE is in each target’s native score scale.

Model	Target	Stat	P_k	r	Params	SRCC	NDCG@5	MAE	
SDXL	HPSv2	E	4	2	1.11M	0.663	0.611	0.0250	
		Esm	4	1	1.90M	0.656	0.613	0.0250	
		E	8	2	1.16M	0.641	0.618	0.0259	
		Esm	8	1	1.95M	0.633	0.616	0.0259	
		E	16	2	1.36M	0.606	0.619	0.0273	
		Esm	16	1	2.15M	0.602	0.624	0.0265	
	PickScore	PickScore	E	4	2	1.11M	0.598	0.607	0.899
			Esm	4	1	1.90M	0.590	0.606	0.917
			E	8	2	1.16M	0.589	0.604	0.905
			Esm	8	1	1.95M	0.577	0.606	0.923
			E	16	2	1.36M	0.563	0.607	0.939
			Esm	16	1	2.15M	0.565	0.606	0.938
PixArt- Σ	HPSv2	E	4	2	2.09M	0.623	0.610	0.0273	
		Esm	4	1	5.17M	0.639	0.597	0.0267	
		E	8	2	2.14M	0.604	0.594	0.0283	
		Esm	8	1	5.21M	0.648	0.588	0.0266	
		E	16	2	2.34M	0.610	0.592	0.0278	
		Esm	16	1	5.41M	0.625	0.588	0.0272	
	PickScore	PickScore	E	4	2	2.09M	0.642	0.572	0.943
			Esm	4	1	5.17M	0.618	0.583	0.977
			E	8	2	2.14M	0.614	0.583	0.978
			Esm	8	1	5.21M	0.601	0.579	1.007
			E	16	2	2.34M	0.596	0.581	0.999
			Esm	16	1	5.41M	0.614	0.570	0.974

Table 9: Prompt/noise budget ablation under a fixed 100,000-sample training set. Bold marks the budget used in the main paper.

Prompts	Noises/prompt	Total	NDCG@5	NDCG@10	SRCC	MAE
1,000	100	100K	0.3202	0.3299	0.0092	2.3727
2,000	50	100K	0.4282	0.4466	0.0059	2.5035
5,000	20	100K	0.6275	0.6636	0.0098	0.811
10,000	10	100K	0.5976	0.7935	-0.0048	1.1917

Table 10: Metric-agreement counts for SDXL PickScore-trained predictors on 100 Pick-a-Pic prompts. Each row reports the number of prompts, out of 100, for which the predictor-selected image improves over the Standard baseline under every metric in the listed set.

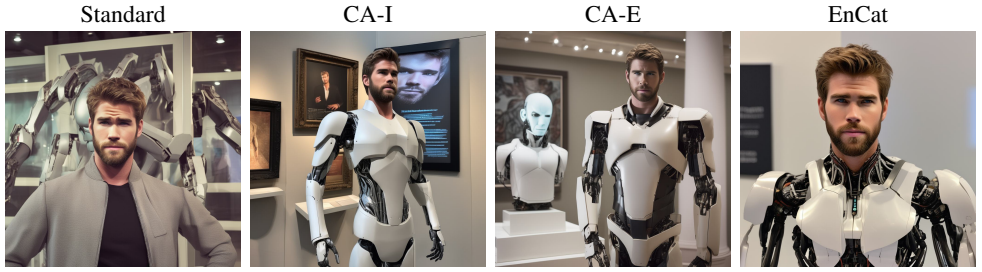
Human Preference Metrics	CA-I	CA-E	EnCat
HPSv2	50	53	55
HPSv3	52	55	58
PS	48	51	54
IR	42	44	46
HPSv2 + HPSv3	35	38	40
HPSv2 + PS	33	35	37
HPSv3 + PS	34	36	39
HPSv2 + IR	27	29	31
HPSv3 + IR	28	30	32
PS + IR	26	28	30
HPSv2 + HPSv3 + PS	26	28	30
HPSv2 + HPSv3 + IR	19	21	23
HPSv2 + PS + IR	18	20	22
HPSv3 + PS + IR	20	22	24
All	13	15	17

B.3 Metric Agreement for PickScore-Trained Predictors

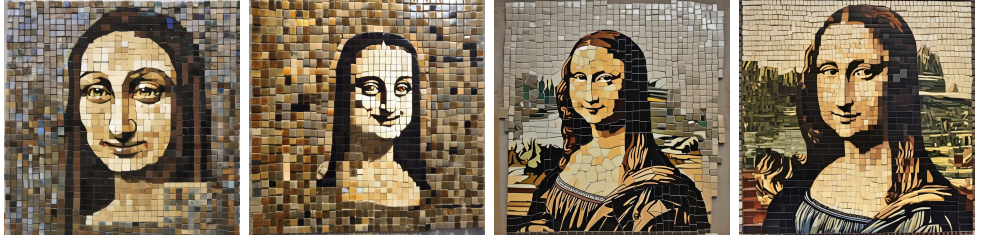
Table 10 reports the metric-agreement counts for the SDXL predictors trained on PickScore, the counterpart to the HPSv2 table in the main paper (Table 4). The same pattern holds: EnCat and CA-E preserve higher agreement than CA-I, and ImageReward remains the least concordant metric.

C Additional Qualitative Examples

We provide additional qualitative examples on SDXL and PixArt- Σ in Fig. 5. Consistent with the quantitative results, CA-E and EnCat track the prompt more coherently than the Standard baseline and CA-I. They render the half-robot, half-humanoid android, place both the woman *and* the dog together on a tree, and seat a rider on the motorcycle, whereas the Standard and CA-I selections more often drop a requested element or produce an awkward composition. Across rows, the noises selected by CA-E and EnCat yield images that are both more prompt-faithful and more visually coherent.



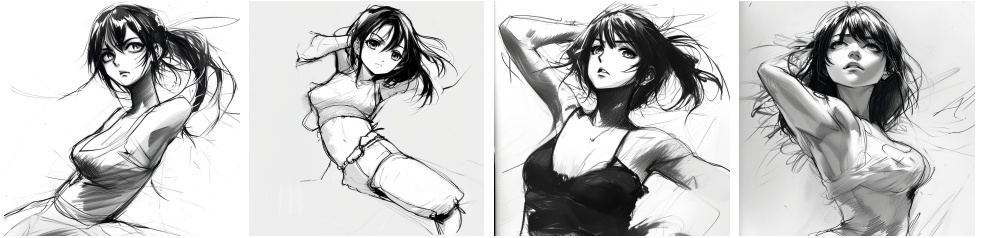
SDXL: “A photo of a male android, half robot and half humanoid, resembling actor Liam Hemsworth, posing stoically on display at a museum.”



SDXL: “A ceramic glass mosaic depicts Mona Lisa’s smile.”



SDXL: “A woman and her dog sit on a tree and watch the sunset in a digital painting by artgerm, greg rutkowski, and Alphonse Mucha”



PixArt-Σ: “Sketch of manga girl in dramatic pose.”



PixArt-Σ: “Yellow and red motorcycle with a man riding on it next to grass.”

Figure 5: Additional qualitative image examples.